



HAL
open science

Ultra-Accurate Correlation between Precursor and Fragment Ions in Two-Dimensional Mass Spectrometry: Acetylated vs Trimethylated Histone Peptides

Michael Palasser, Sarah V Heel, Marc-André Delsuc, Kathrin Breuker, Maria A van Agthoven

► **To cite this version:**

Michael Palasser, Sarah V Heel, Marc-André Delsuc, Kathrin Breuker, Maria A van Agthoven. Ultra-Accurate Correlation between Precursor and Fragment Ions in Two-Dimensional Mass Spectrometry: Acetylated vs Trimethylated Histone Peptides. *Journal of The American Society for Mass Spectrometry*, 2023, 34 (4), pp.608 - 616. 10.1021/jasms.2c00319 . hal-04959084

HAL Id: hal-04959084

<https://hal.science/hal-04959084v1>

Submitted on 20 Feb 2025

HAL is a multi-disciplinary open access archive for the deposit and dissemination of scientific research documents, whether they are published or not. The documents may come from teaching and research institutions in France or abroad, or from public or private research centers.

L'archive ouverte pluridisciplinaire **HAL**, est destinée au dépôt et à la diffusion de documents scientifiques de niveau recherche, publiés ou non, émanant des établissements d'enseignement et de recherche français ou étrangers, des laboratoires publics ou privés.



Distributed under a Creative Commons Attribution 4.0 International License

Ultra-Accurate Correlation between Precursor and Fragment Ions in Two-Dimensional Mass Spectrometry: Acetylated vs Trimethylated Histone Peptides

Michael Palasser, Sarah V. Heel, Marc-André Delsuc, Kathrin Breuker, and Maria A. van Agthoven*




Cite This: *J. Am. Soc. Mass Spectrom.* 2023, 34, 608–616



Read Online

ACCESS |

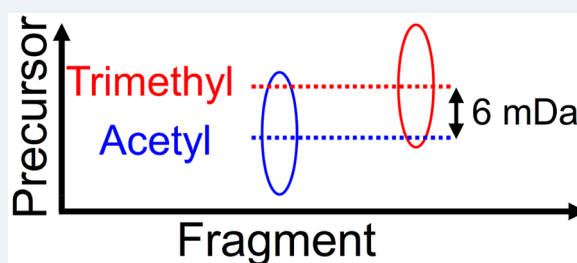
 Metrics & More

 Article Recommendations

 Supporting Information

ABSTRACT: Two-dimensional mass spectrometry (2D MS) is a method for tandem mass spectrometry in which precursor and fragment ions are correlated by manipulating ion radii rather than by ion isolation. A 2D mass spectrum contains the fragmentation patterns of all analytes in a sample, acquired in parallel. We report ultrahigh-resolution narrowband 2D mass spectra of a mixture of two histone peptides with the same sequence, one of which carries an acetylation and the other a trimethylation (m/z 0.006 difference). We reduced the distance between data points in the precursor ion dimension and compared the accuracy of the precursor-fragment correlation with the resolving power.

We manage to perform label-free quantification on the histone peptide mixture and show that precursor and fragment ions can be accurately correlated even though the precursor ions are not resolved. Finally, we show that increasing the resolution of a 2D mass spectrum in the precursor ion dimension too far can lead to a decline in the signal-to-noise ratio.



INTRODUCTION

In tandem mass spectrometry, ions undergo fragmentation to yield structural information beyond the measurement of their mass-to-charge (m/z) ratio. For complex samples, one of the most important issues is the correlation between fragment ions and their precursors. In most standard applications, this correlation is achieved by isolating a single ion species before fragmentation.¹ With highly complex samples, ion isolation needs to be performed with narrow m/z windows, which can be challenging. To date, stored-waveform inverse Fourier transform and correlated harmonic excitation fields isolation are the two methods that offer the narrowest m/z windows in ion isolation.^{2–5}

Two-dimensional mass spectrometry (2D MS) correlates precursor and fragment ions by manipulating their trajectories, typically in a quadrupolar ion trap or in an ion cyclotron resonance (ICR) cell.^{6–11} Other methods such as two-dimensional partial covariance mass spectrometry (2D PC MS) correlate fragment ions with one another.^{12–14} Because 2D MS does not require ion isolation and relies on signal multiplexing, it can measure the structural information on analytes in complex samples in a parallel instead of in a serial way.⁶

The pulse sequence for 2D FT-ICR MS (two-dimensional Fourier transform ion cyclotron resonance mass spectrometry) was developed by Pfändler et al. and has been optimized for various fragmentation methods, such as infrared multiphoton dissociation, electron capture dissociation (ECD), infrared-activated ECD, electron-induced dissociation, and ultraviolet

dissociation.^{15–21} Programs have been developed for data processing and analysis, and algorithms have been developed for noise reduction.^{6,22–24} Applications for 2D MS include small molecules, proteomics (bottom-up and top-down), polymer analysis, and agrochemicals.^{20,21,25–32} A narrowband method has been developed for high resolution precursor-fragment correlation over small m/z ranges as well as strategies for phase correction to improve both the resolving power and the signal-to-noise ratio of 2D mass spectra.^{33–35}

Recent studies by Marzullo *et al.* and by Paris *et al.* show that precursor and fragment ions can be correlated accurately, even for multiple precursor ions peaks that are not properly resolved in the vertical precursor ion dimension.^{21,31} In this study, we performed narrowband 2D MS on an FT-ICR mass spectrometer, in phase-corrected absorption mode, on the mixture of trimethylated and acetylated forms of histone peptide with an m/z difference of 0.006. We varied the frequency range in the precursor ion dimension and compared the resolving power, signal-to-noise, and precursor-fragment correlation to probe the limits of performance of 2D MS in terms of accurate precursor-fragment correlation.

Received: November 13, 2022

Revised: January 23, 2023

Accepted: March 8, 2023

Published: March 17, 2023



Here, we define resolution of a spectrum as the distance between two adjacent data points, resolution of a peak as its full-width at half-maximum (FWHM), resolving power as the measurement of a peak centroid divided by the FWHM of the peak, and precursor-fragment correlation as the capacity to accurately assign both a precursor and a fragment ion for a peak in a 2D mass spectrum.

EXPERIMENTAL METHODS

Sample Preparation. Milli-Q water (Merck Millipore, Darmstadt, Germany), methanol, and acetic acid (VWR, Vienna, Austria) were used in all experiments. C-terminal GK-biotinylated histone H3 sequences (amino acid residues 21–44) with native modifications (acetylation at K27 and trimethylation at K36) were purchased (AnaSpec, Fremont, CA, USA) with a purity of >95%, in which K27 of the full-length histone corresponds to K7 of the model peptides and K36 in the histone corresponds to K16 in the peptides.

Peptides were desalted using MWCO 2000 Vivaspin centrifugal concentrators (Sartorius, Göttingen, Germany) at 7900 rcf, 6× ammonium acetate 100 mM (Sigma, Vienna, Austria), and 6× H₂O. Peptide concentration was determined by UV absorption at 280 nm using an Implen Nano Photometer™ (Implen, München, Germany). For electrospray ionization, equimolar mixtures (0.2 μM each) of acetylated and trimethylated peptides (referred to as “K7 Ac” and “K16 3m”, respectively, in the text) in 50:50 H₂O/CH₃OH and 1% vol CH₃COOH, pH ~ 3.0 were prepared from 100 μM stock solutions of each peptide in H₂O.

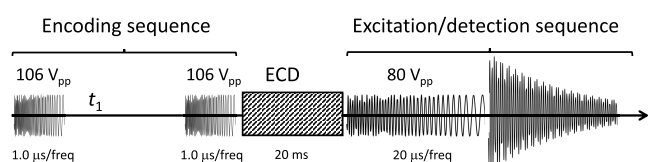
Instrument Parameters. All mass spectra were acquired on a 7 T Apex Ultra FT-ICR mass spectrometer (Bruker Daltonik, GmbH, Bremen, Germany) with an electrospray ion source operated in positive mode and direct injection at a flow rate of 70 μL/h.³⁶ Ions were transferred to the Infinity ICR cell through a series of focusing lenses.³⁷

The mass spectrum of the histone peptide mixture was recorded over 20 scans with a 2 M data point transient (2.93 s) after ion accumulation of 0.1 s in the first hexapole and transfer to the second hexapole. The mass range was m/z 303.3–1500 (corresponding to a frequency range of 357.143–72.171 kHz). The excitation sweep had an amplitude of 80 V_{pp} with 20 μs/frequency (each frequency step is 624.64 Hz).

The four 2D mass spectra were acquired after ion accumulation of 0.2 s in the first hexapole and transfer to the second hexapole. Ions were isolated in the quadrupole at m/z 494 with an isolation window of m/z 30. The fragmentation method was ECD with a hollow cathode, with the heater set at 1.2 A, the lens at 20 V, the bias at 2.0 V, and the irradiation at 20 ms.³⁸

The pulse sequence for the 2D MS experiment is shown in Scheme 1. The two pulses in the encoding sequence were set at 106 V_{pp} amplitude with 1.0 μs/frequency, and the pulse in the excitation/detection sequence was set at 80 V_{pp} amplitude with a 20 μs/frequency (each frequency step is 624.64 Hz).

Scheme 1. Pulse Sequence for 2D Mass Spectrometry



These parameters were optimized with the same method that has been discussed in previous articles.^{18,19} The encoding delay t_1 was incremented 1024 times in each experiment. Transients were acquired over 1 scan per value of t_1 with 512 k data points (0.734 s). All pulses in the pulse sequence have the same frequency range. All four 2D mass spectra were acquired in narrowband mode, with different frequency ranges for the encoding and excitation pulses to provide for the desired frequency range in the final 2D mass spectra.³⁵ All these parameters are shown in Table 1. For a detailed explanation of narrowband mode 2D MS, see Scheme S1 in the Supporting Information.

Four MS/MS spectra were acquired for use in determining the coefficients of the horizontal quadratic phase correction function with the same frequency ranges as the 2D mass spectra listed in Table 1. The front-end conditions, ECD parameters, and transients of these MS/MS spectra were identical to the ones in the 2D mass spectrum. The MS/MS spectra were acquired with 500 accumulated scans each.

Data Processing. Both the one-dimensional (1D) and 2D mass spectra were processed and visualized using the Spectrometry Processing Innovative Kernel (SPIKE) software (available at www.github.com/spike-project, accessed on June 1, 2021) developed by the University of Strasbourg (Strasbourg, France) and CASC4DE (Illkirch-Graffenstaden, France) in the 64-bit Python 3.7 programming language on an open-source platform distributed by the Python Software Foundation (Beaverton, OR, USA).²² Processed data files were saved using the HDF5 file format.

The 1D mass spectra were apodized with a square sine-bell window with a maximum at 0.15 and zero-filled to 4096 data points before Fourier transformation and quadratic phase-correction and baseline correction. The 2D mass spectra were digitally demodulated, apodized with a sine-bell window with a maximum at 0.15, zero-filled twice, denoised with the SANE algorithm (with a rank of 30), and phase-corrected quadratically along the horizontal axis and linearly along the vertical axis, before the frequencies were offset to recalculate the original frequency range in the vertical dimension.^{23,24,34,35} The size of the resulting data sets was 1,048,576 data points horizontally (fragment ion dimension) by 2048 data points vertically (precursor ion dimension).

Peak-picking for fragment assignments and relative quantification was achieved by extracting horizontal fragment ion scans for each precursor isotope and baseline-correction before accumulation. Peak-picking was conducted on the resulting data set, followed by centroiding and frequency-to-mass quadratic internal conversion.³⁹ To determine the correlation between precursor and fragment ions, we peak-picked by extracting the horizontal fragment ion scan of the M or M+1 isotope of the precursor ion. Then the vertical precursor ion scan at the peak was extracted, baseline-corrected, and peak-picked. Each peak was centroided (polynomial fit). The 1D profile data from the vertical precursor ion scans and the centroid were used to generate a Lorentzian fit. All programs used are listed in the Supporting Information.

RESULTS AND DISCUSSION

Scheme 1 shows the pulse sequence for 2D MS on an FT-ICR mass spectrometer.^{15–17} During the encoding sequence, precursor ion radii are modulated. The first pulse increases the radius of all precursor ions, after which they are left to rotate at their cyclotron frequency during the encoding delay

Table 1. Experimental Conditions of the 2D Mass Spectra

Nyquist frequency (kHz)	t_1 increment (μ s)	Frequency range of all pulses (kHz)	Horizontal m/z range	Number of foldovers	Vertical m/z range
10	50	357.143–74.660	303.3–1450	14	482.011–504.438
4	125	357.143–72.171	303.3–1500	36	491.828–500.916
2	250	357.143–73.895	303.3–1465	72	492.438–496.952
1	500	357.143–74.402	303.3–1455	144	493.539–495.796

(t_1). The ions accrue phase, which brings them out of phase with the second pulse and leads to radius modulation according to the ions' cyclotron frequency and t_1 .⁴⁰ Because ECD fragmentation is radius dependent, the abundance of the fragment ions is modulated according to t_1 and the cyclotron frequencies of their precursors.⁴¹ The excitation/detection sequence brings all ions to high radius to acquire the transient.⁶

The pulse sequence is repeated for regularly incremented values of t_1 . Each transient is Fourier-transformed. Then the signal for each frequency is Fourier-transformed according to t_1 . After frequency-to-mass conversion, the 2D mass spectrum shows the fragmentation patterns of all analytes in the sample. In each dimension, the spectrum resolution increases with the number of data points and with decreasing frequency ranges.⁴²

Figure 1 shows the sequence (which corresponds to residues 21 to 44 of the histone H3 protein) and modifications of the

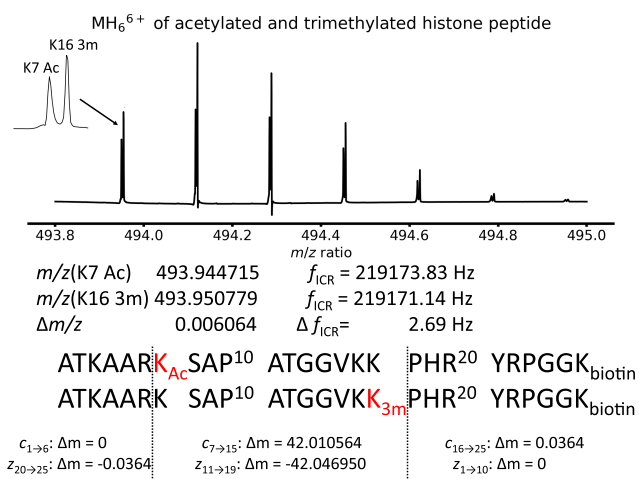


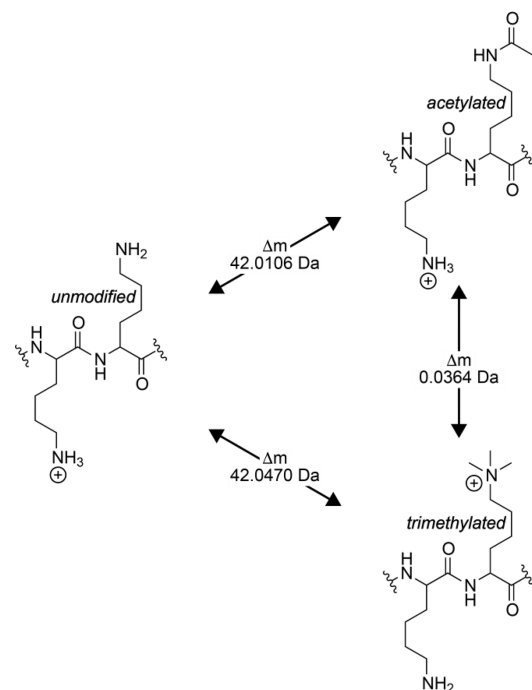
Figure 1. Sequence, m/z ratios, theoretical cyclotron frequencies, and isotope signals of the $[M+6H]^{6+}$ ions of the K7 Ac and K16 3m histone peptides (full spectrum in Figure S1 in the Supporting Information).

two histone peptides used in this study. Both peptides are biotinylated at K26, in addition to which one is acetylated at lysine 7 (K7 Ac) and the other trimethylated at lysine 16 (K16 3m). The mass difference between the two histone peptides is 36 mDa.

Figure 1 shows the isotopic distribution of the $[M+6H]^{6+}$ ions in the 1D mass spectrum of a $\sim 1:1$ mixture of the two histone peptides (full spectrum in Figure S1 in the Supporting Information). The mass spectrum was acquired with 2 M data points and a Nyquist frequency of 357.143 kHz (the length of the transient was 2.936 s). Processing was achieved with two zero-fills in phase-corrected absorption mode. The peaks of the K7 Ac and K16 3m peptides (which are separated by m/z 0.006 or 2.7 Hz in cyclotron frequency at $z = 6$) are nearly baseline-resolved.

Scheme 2 illustrates mass differences (Δm) between unmodified, acetylated, and trimethylated fragments, according

Scheme 2. Mass Differences between Unmodified, Acetylated, and Trimethylated Fragments



to which fragments can be separated into three different categories: 1) fragments without any modified residues, 2) fragments with mass values which are ~ 42 Da higher than for a peptide without modification (i.e., 42.0106 Da for acetylation and 42.047 Da for trimethylation), and 3) fragments whose mass values differ by 36.4 mDa (trimethylation versus acetylation). We can use these three categories to study how accurately the precursor and fragment ions can be correlated in 2D MS.

Figure 2a shows the 2D mass spectrum of the $[M+6H]^{6+}$ ions of the equimolar mixture of K7 Ac and K16 3m with a frequency range of 10 kHz in phase-corrected absorption mode. A previous study has shown that the isotopic pattern of $[M+6H]^{6+}$ ions of methylated histone peptides is baseline-resolved in the vertical precursor ion dimension.³⁴ The frequency difference between two adjacent data points (or resolution) in the vertical dimension is 4.9 Hz. Moreover, the maximum value of t_1 in this experiment is 51.2 ms, which means that the minimum frequency resolution of each peak is 19.5 Hz. Therefore, the signals from the two histone peptide ions, which have a modulation frequency difference of 2.7 Hz, cannot be resolved.

The fragment ion scans for the M, M+1, M+2, and M+3 isotopes were extracted from the 2D mass spectrum and added up to reconstitute an "added-up spectrum" that is equivalent to

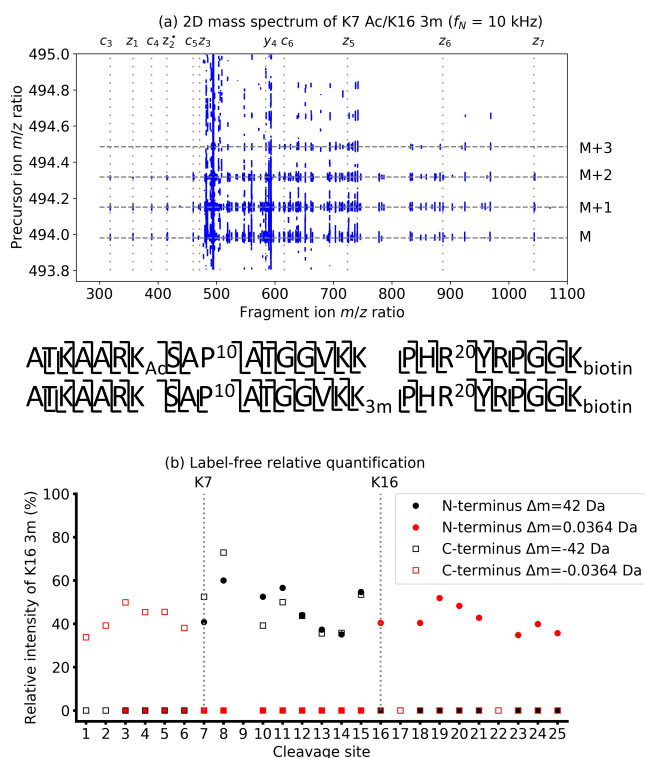


Figure 2. (a) Phase-corrected absorption mode 2D mass spectrum of the K7 Ac/K16 3m histone peptide mixture and sequence coverage of the two peptides. (b) Label-free relative quantification of the two histone peptides using the relative abundances of their fragment ion peaks.

a standard tandem mass spectrum with quadrupole isolation of the entire isotopic distribution of the precursor (see Figure S2 in the Supporting Information). Because in narrowband mode 2D MS the fragment ion scans of the isotopes are not adjacent to each other (unlike the fragment ion scans of the different isotopes in a broadband 2D mass spectrum), the noise signals are not correlated between them. Adding up the fragment ion scans there increased the signal-to-noise ratio in the added-up spectrum.

We peak-picked the added-up spectrum and assigned the fragment ion peaks, which lead to a 96% sequence coverage for each histone peptide, as shown in Figure 2 (the full list of assigned fragment peaks is shown in Table S1 of the Supporting Information).

Figure 2b shows the label-free relative quantification of the two histone peptides using the relative intensities in the added-up spectrum. In a previous study, 2D MS was used for label-free relative quantification of histone peptides with 0–3 methylations on the K7 residue.³⁵ Their m/z ratios were clearly separated in the vertical precursor ion dimension, which made information on the difference in m/z ratios between

fragment ion peaks redundant. Here we cannot resolve the two histone peptides in the vertical precursor ion dimension, so the information provided by fragment ion m/z ratios is necessary. Therefore, we calculated and plotted the results of the label-free relative quantification in the same way as in standard tandem mass spectrometry, by using the mass differences between the fragments ions of the two histone peptides (horizontal fragment ion dimension).⁴³ As illustrated in Figure 2b, the information that one histone peptide is acetylated at K7 and the other trimethylated at K16 was recovered.

To determine parameters for accurate correlation between fragments of K7 Ac and K16 3m and their precursors, we acquired 2D mass spectra with frequency ranges varying between 1 and 10 kHz, with all other parameters remaining identical. As mentioned before, the spectrum resolution (or Hz per point) in the vertical precursor ion dimension is 4.9 Hz for a 10 kHz frequency range. The spectrum resolution is 2.0 Hz for a 4 kHz frequency range, 1.0 Hz for a 2 kHz frequency range, and 0.5 Hz for a 1 kHz frequency range. Furthermore, the maximum value of t_1 is 128 ms for a 4 kHz frequency range, leading to a minimum peak resolution of 7.8 Hz. For a 2 kHz frequency range, the minimum peak resolution is 3.9 Hz, and 2 Hz for a 1 kHz frequency range. Since the difference in modulation frequency between the two precursor ions is 2.7 Hz, we expect the correlation between precursor and fragment ion peaks to improve with narrowing frequency ranges. Table 2 illustrates how the performance of the analysis evolved with the narrowing frequency range.

Table 2 shows that the total duration of the experiment increased by almost 4 min by reducing the frequency range from 10 kHz to 1 kHz. The duration T of the acquisition of a 2D MS data set can be expressed as

$$T = N(T_{acc} + T_{transfer} + T_{pulses} + T_{irradiation} + T_{delays} + T_{detect}) + \frac{N(N+1)}{2} \Delta t_1 \quad (1)$$

in which T_{acc} is the total duration of the accumulation of the ions in the mass spectrometer, $T_{transfer}$ the duration of ion transfer through the ion optics, $T_{irradiation}$ the duration of fragmentation, T_{pulses} the duration of all the pulses applied on the excitation plates, T_{delays} the total duration of instrument delays, T_{detect} the length of the transient, and N is the number of increments of the encoding delay Δt_1 (see Scheme 1). The sum of these durations is on the order of 1 s. The increment Δt_1 is almost on the order of 1 ms and increases with N^2 (or in $O(N^2)$) and should be considered for experiment design and sample consumption.

Figure 3 shows the evolution of the intensity of the precursor ion peak of the K7 Ac histone peptide (mono-isotopic peak at m/z 493.9466) with the encoding delay t_1 extracted from the 2D mass spectrum with a 1 kHz frequency range. The modulation of the precursor ion radius is observed

Table 2. Comparison in Performance between 2D Mass Spectra with Narrowing Frequency Ranges

Frequency range (kHz)	Experiment duration (min)	max. t_1 (ms)	Vertical resolving power (z_5 fragment)	Signal-to-noise ratio (z_5 fragment)	Vertical resolving power ($z(K7Ac)_{13}^{3+}$ fragment)	Signal-to-noise ratio ($z(K7Ac)_{13}^{3+}$ fragment)	Number of assigned fragments
10	23.63	51.2	13,700	94	13,700	60	132
4	24.28	128	22,500	60	22,500	66	121
2	25.35	256	27,400	34	33,000	35	83
1	27.56	512	27,400	11	N/A	N/A	84

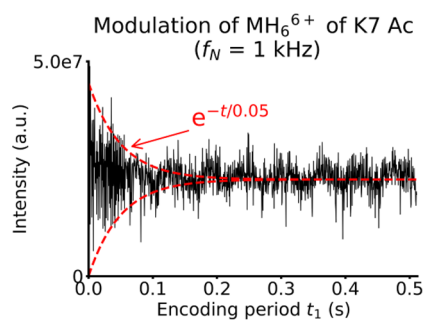


Figure 3. Evolution of the intensity of the $[M+6H]^{6+}$ precursor ion of the K7 Ac histone peptide with the encoding period t_1 after data processing in the horizontal dimension, extracted from the 2D mass spectrum with a 1 kHz frequency range (black). Theoretical exponential decay functions with a decay rate of 20 s^{-1} (red).

through the variation of the intensity of the peak, which decreases rapidly when t_1 increases. In red dashed lines, we superimposed an exponential decay with a half-life of 50 ms, which corresponds to the envelope of the intensity of the precursor. Therefore, we can estimate that the decay rate of the ion packet has a characteristic time of approximately 50 ms.

Theoretical studies and particle-in-cell simulations have shown that various factors (e.g., Coulombic repulsion or electric fields from the ICR cell electrodes) cause loss of coherent ion motion.^{44–46} In the 2D MS experiments presented here, narrowing the frequency range in the vertical dimension results in longer encoding delays after the first encoding pulse (see Scheme 1).

Loss of coherent ion motion is likely to happen when t_1 is increased. Precursor ion radius modulation is heavily dependent on the coherence of the ion packet at the end of the encoding delay, and therefore decreases in amplitude when t_1 increases too much.⁴⁰ This phenomenon explains why the signal-to-noise ratio decreases with narrower frequency ranges and why the vertical resolving power fails to increase as expected. An increase in pressure during the experiment would also lead to loss of coherence for ion packets, but this would be dependent on experiment duration and not on t_1 , and would be evident from peak broadening in the horizontal fragment ion dimension.

Both K7 Ac and K16 3m have the same z_5 fragment (see Figure 1 and Scheme 2). Figure 4 shows the precursor ion scans for z_5 for all four 2D mass spectra. The resolution of the peaks goes from m/z 0.036 mDa at 10 kHz (Figure 4a) to m/z 0.022 at 4 kHz (Figure 4b) and m/z 0.018 at 2 kHz (Figure 4c).⁴² In the 2D mass spectrum with a 1 kHz frequency range (Figure 4d), the peaks for the K7 Ac and the K16 3m precursors start to become resolved. For the 1 kHz frequency range, the spectrum resolution in the frequency domain is 0.5 Hz, while the difference in frequency modulation between the two precursors is 2.7 Hz. Therefore, in Figure 4d the peaks are sufficiently well-defined to allow them to be both detected. However, Figure 4 also illustrates that the signal-to-noise ratio decreases with the frequency range, as has been discussed previously: in Figure 4a and Figure 4b, four isotopic peaks of the precursor ions can be detected, but in Figure 4c only three are detected and in Figure 4d only two are detected. In Figure 4d, the noise structure is characteristic of residual noise after SANE denoising.²⁴

Fragment z_{13}^{3+} is modified for the K16 3m peptide, but not for K7 Ac. In each 2D mass spectrum, the two vertical

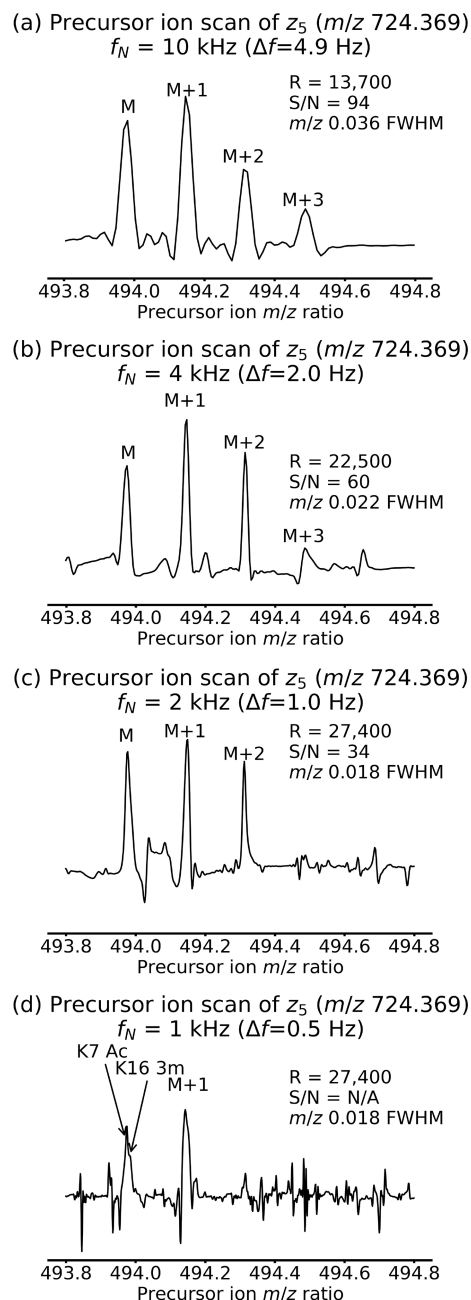


Figure 4. Precursor ion scans for fragment z_5 of both K7 Ac and K16 3m histone peptide extracted from 2D mass spectra with $f_N =$ (a) 10 kHz frequency range, (b) 4 kHz frequency range, (c) 2 kHz frequency range, and (d) 1 kHz frequency range. R: resolving power, S/N: signal-to-noise ratio, FWHM: full width at half-maximum.

precursor ion scans are separated by m/z 14.0157, and they can therefore be used to examine the separation between the signals from the two histone peptides (see Figure 1 and Scheme 2). Figure 5 shows the normalized precursor ion scans of the z_{13}^{3+} fragment of both histone peptides extracted from the 2D mass spectra with 10 kHz (Figure 5a), 4 kHz (Figure 5b), and 2 kHz (Figure 5c) precursor ion frequency range. This fragment ion was not detected at a sufficient signal-to-noise ratio for either histone peptide in the 2D mass spectrum with a precursor ion frequency range of 1 kHz.

When comparing Figure 5a–c, we see that the vertical FWHM of the peaks decreases from approximately m/z 0.039

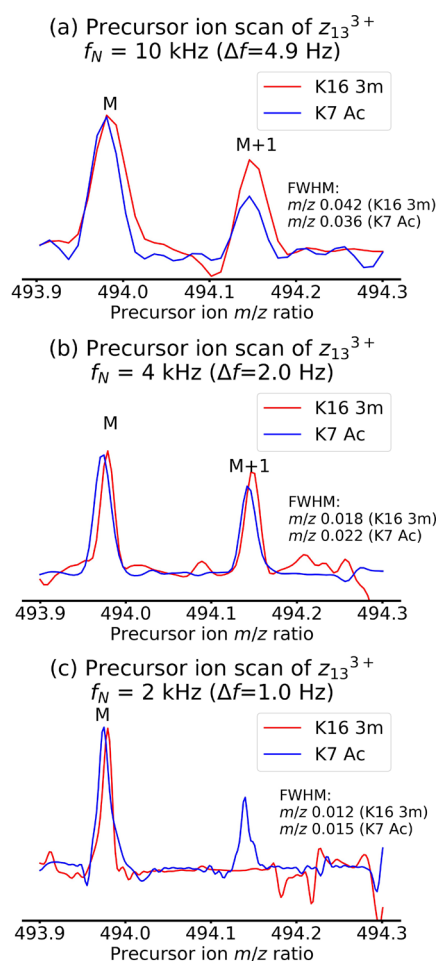


Figure 5. Normalized precursor ion scans for fragment z_{13}^{3+} of both K7 Ac (m/z 563.978366) and K16 3m (m/z 577.996078) histone peptide extracted from 2D mass spectra with (a) 10 kHz frequency range, (b) 4 kHz frequency range, and (c) 2 kHz frequency range.

for a frequency range of 10 kHz to m/z 0.014 for 2 kHz. This decrease is consistent with the decrease in frequency range. However, the vertical FWHM decrease by a factor of 2.6 instead of 5 as expected from the decrease in frequency ranges. We also notice a reduction in the signal-to-noise ratio from Figure 5a–c. In Figures 5a and 4b, the M+1 isotopic peak is detected, but not in Figure 5c (see also Table 2). These observations are observed in the vertical precursor ion dimension, which reflects behavior as a function of t_1 , and are consistent with loss of coherence in ion motion during the encoding delay as discussed above.

Although the peaks are too broad to be properly resolved, we notice that the peak for K16 3m is consistently shifted to higher m/z ratios compared to K7 Ac. There is more overlap between the two peaks in Figure 5a than in Figure 5b,c. In Figure 5b,c, this result is consistent with the difference in modulation frequency between the two histone peptides, which is 2.7 Hz.

The M+1 isotopic peak is detected for both histone peptides in Figure 5a,b, and the shift in m/z ratio between the two precursor ion scans is also evident. In the M+1 isotopic peak, the contribution of ^2H , ^{15}N , ^{17}O , and ^{33}S (the sulfur is in the biotinylation) is about 13% of the total abundance of the M+1 peak and corresponds to a mass difference of over 9 mDa (see Tables S5 and S6 in the Supporting Information). Therefore,

the M+1 isotopic peak corresponds to multiple isotopologues (^{13}C , ^2H , ^{15}N , ^{17}O , ^{33}S) with mass differences that are of the same order of magnitude as the mass difference between K7 Ac and K16 3m, instead of one isotopologue (^{12}C , ^1H , ^{14}N , ^{16}O , ^{32}S), which is a cause of peak shift. Therefore, using the M+1 isotopic peak to detect the peak shift between K7 Ac and K16 3m is not as accurate as using the monoisotopic peak.

Figure 6 shows box-plot representations of the positions of the fragment ion peaks in the vertical precursor ion scans (in the frequency domain) after a Lorentzian linefit for the c_{7-15} and y/z_{11-18} fragments, for both histone peptides, extracted from the 2D mass spectrum with a 10 kHz (Figure 6a), 4 kHz (Figure 6b), and 2 kHz (Figure 6c) frequency range.

Between the plots, the frequency range of the peaks shifts by approximately 6 Hz (219,268–219,276 Hz in Figure 6a and 219,275–219,281 Hz in Figure 6c). This variation is due to the fact that the lowest frequency in the excitation pulses was adjusted for each 2D MS experiment (see Table 1), and there is a slight imprecision in the Bruker metadata.³⁵ We also notice that the number of data points decreases when the frequency range becomes narrower, which is consistent with the decrease in signal-to-noise with narrowing frequency range shown in Table 2.

The vertical frequencies measured for the fragments of K16 3m and K7 Ac form two distinct populations centered around average frequencies that differ by 2.1 Hz for a 10 kHz frequency range, 2.7 Hz for a 4 kHz frequency range, and 2.0 Hz for a 2 kHz frequency range, which is consistent with the theoretical difference in cyclotron frequency between the $[M+6\text{H}]^{6+}$ ions of the two histone peptides (see Figure 1). For the 2D mass spectra with a 10 kHz and a 2 kHz frequency range, there is a partial overlap between the fragments of K16 3m and the fragments of K7 Ac, but not for the 2D mass spectrum with a 4 kHz frequency range. This result is likely due to two competing factors. On the one hand, narrowing the frequency range improves the accuracy of the frequency measurement because the data points are closer to each other. On the other hand, the reduction in signal-to-noise ratio, which is caused by longer values of the encoding delay t_1 (see Scheme 1), induces errors in the frequency measurement.

The same analysis was performed for the c_{16-25} and y/z_{19-25} fragments of the M isotopes of the two histone peptides (see Figure S6 in the Supporting Information), which are only separated by 0.0364 Da horizontally (see Figure 1), and for the c_{7-15} and y/z_{11-18} fragments of the M+1 isotopes of the two histone peptides (see Figure S7 in the Supporting Information), in which multiple isotopologues overlap. In both cases, the two ion populations could not be distinguished properly, which shows that peaks overlapping causes errors in the measurement.

CONCLUSION

In this study, we performed phase-corrected narrowband 2D MS on the mixture of an acetylated histone peptide and a trimethylated histone peptide. With a 10 kHz frequency range in the vertical precursor ion dimension, the distance between data points in the vertical dimension of the final 2D mass spectrum was nearly twice the difference in cyclotron frequency between the two precursor ions. Nevertheless, we not only achieved nearly complete sequence coverage of both histone peptides and relative quantification of the modifications but also managed nearly complete correlation of fragments with their precursor ions. Narrowing the frequency

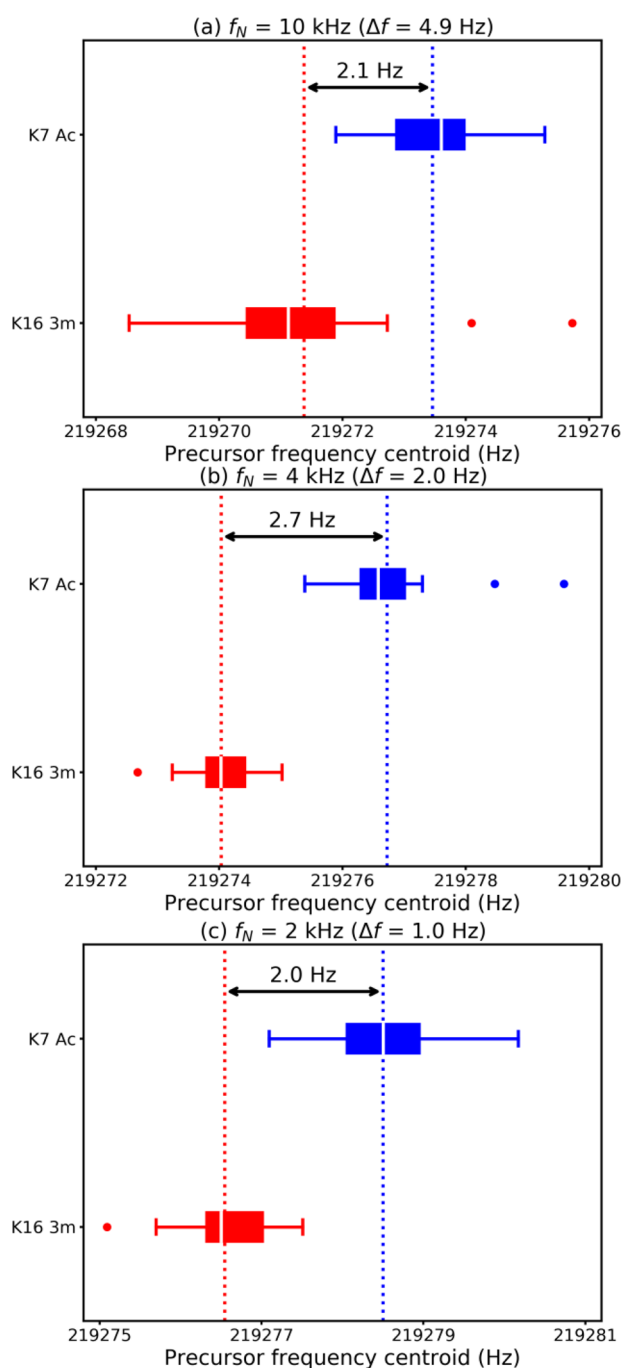


Figure 6. Distribution of frequencies of fragment ion peaks (vertical precursor ion dimension) after Lorentzian fit for fragment ions c_{7-15} and y/z_{11-18} of the K16 3m (red) and the K7 Ac (blue) histone peptides (M isotopic peaks only). The vertical dotted lines indicate the average frequency (arithmetic mean) measured for the fragments of K16 3m (red) and K7 Ac (blue). The medians are indicated in white in the boxplots. These measurements were performed on the 2D mass spectra acquired with (a) 10 kHz frequency range, (b) 4 kHz frequency range, and (c) 2 kHz frequency range.

range in the vertical dimension, with all other parameters remaining equal, made the correlation more accurate, but only to a certain point. Narrowing the frequency range lead to longer encoding delays in the pulse sequence to the point where ion packets lost coherence. As a result, the precursor ion radius modulation was decreased, and therefore the signal-to-

noise ratio of the fragment ion peaks in the 2D mass spectrum decreased.

Until now, the vertical resolving power has been used as a measure of the accuracy of the precursor-fragment correlation in 2D MS. This study shows that the vertical resolving power underestimates the precursor-fragment correlation. Our new results show that a more accurate measurement of the precursor-fragment correlation is less than the difference between two data points in the vertical dimension.

To increase the precursor-fragment correlation even further, ICR cells that have been designed to keep ion packets coherent for longer time periods, such as the electrically compensated or the dynamically harmonized cell, can be used, as has already successfully been done in 1D FT-ICR MS.^{47–50} We can also increase precursor-fragment correlation by decreasing the minimum distance between data points nonuniform sampling.²⁴ Finally, we can move beyond the Fourier transform in the vertical dimension for data processing methods that yield more accurate frequency measurements, such as the filter diagonalization method.^{51–53} This study shows that 2D MS is a useful analytical tool for tandem mass spectrometry studies of isobaric species with the same charge state. Beyond modified peptides and proteins, 2D MS is shown here to be a viable alternative for the structural analysis of environmental samples, for which the isolation of a single ion species can be extremely challenging.⁵ Recording 2D mass spectra for different segments of the precursor ion m/z range can lead to accurate structural information of every analyte in a sample with a high degree of confidence, even if the precursor ions are not resolved in the vertical dimension.

■ ASSOCIATED CONTENT

Data Availability Statement

All raw data files available at: <https://zenodo.org/record/7741445#.ZBNIAHbMLGh>.

Supporting Information

The Supporting Information is available free of charge at <https://pubs.acs.org/doi/10.1021/jasms.2c00319>.

Detailed explanation of 2D MS; data processing for all 2D MS spectra; baseline correction of fragment ion scans; addition of fragment ion scans and peak-picking; baseline correction of precursor ion scans; peak-picking; and line-fitting of peaks; mass spectrum of the equimolar mixture of the acetylated histone peptide (K7) and the trimethylated histone peptide (K16) in phase-corrected absorption mode; illustration of the process of adding-up horizontal fragment ions scans; peak assignment of all 2D mass spectra theoretical mass and relative abundance of the M and M+1 isotopes of the K7 Ac and K16 3m histone peptides; distribution of frequencies of fragment ion peaks (vertical precursor ion dimension) after Lorentzian fit for fragment ions c_{16-25} and y/z_{19-25} of the K16 3m (red) and the K7 Ac (blue) histone peptides (M isotopic peaks only); distribution of frequencies of fragment ion peaks (vertical precursor ion dimension) after Lorentzian fit for fragment ions c_{7-15} and y/z_{11-18} of the K16 3m (red) and the K7 Ac (blue) histone peptides (M+1 isotopic peaks only) (PDF)

AUTHOR INFORMATION

Corresponding Author

Maria A. van Agthoven – Institute for Organic Chemistry, University of Innsbruck, 6020 Innsbruck, Austria; Present Address: BIOCEV, Institute of Microbiology, Czech Academy of Sciences, Prumyslová 595, 252 50 Vestec, Czech Republic; orcid.org/0000-0003-2438-3934; Email: maria.vanagthoven@biomed.cas.cz

Authors

Michael Palasser – Institute for Organic Chemistry, University of Innsbruck, 6020 Innsbruck, Austria

Sarah V. Heel – Institute for Organic Chemistry, University of Innsbruck, 6020 Innsbruck, Austria

Marc-André Delsuc – Institut de Génétique et de Biologie Moléculaire et Cellulaire, INSERM U596, UMR 7104, Université de Strasbourg, 67404 Illkirch-Graffenstaden, France; CASCADÉ, 67400 Illkirch-Graffenstaden, France; orcid.org/0000-0002-1400-5326

Kathrin Breuker – Institute for Organic Chemistry, University of Innsbruck, 6020 Innsbruck, Austria

Complete contact information is available at: <https://pubs.acs.org/10.1021/jasms.2c00319>

Funding

Open Access is funded by the Austrian Science Fund (FWF).

Notes

The authors declare no competing financial interest.

ACKNOWLEDGMENTS

M.A.v.A. dedicates this article to the memory of Dr. Andreas J. van Agthoven. M.-A.D. thanks Sasha for his help in editing the manuscript. M.A.v.A. thanks Dr. Alan Kádek and Dr. Petr Man for their help editing this article. The authors would like to thank Dr. Christopher A. Wootton for helpful conversations. M.A.v.A. and K.B. thank Der Wissenschaftsfonds (Austrian Science Fund, FWF) for the Lise Meitner Fellowship project M 2757-B.

REFERENCES

- (1) de Hoffmann, E. Tandem mass spectrometry: A primer. *Journal of Mass Spectrometry* **1996**, *31* (2), 129–137.
- (2) de Koning, L. J.; Nibbering, N. M. M.; van Orden, S. L.; Laukien, F. H. Mass selection of ions in a Fourier transform ion cyclotron resonance trap using correlated harmonic excitation fields (CHEF). *Int. J. Mass Spectrom. Ion Process.* **1997**, *165-166*, 209–219.
- (3) O'Connor, P. B.; McLafferty, F. W. High-resolution ion isolation with the ion cyclotron resonance capacitively coupled open cell. *J. Am. Soc. Mass Spectrom.* **1995**, *6* (6), 533–5.
- (4) O'Connor, P. B.; Little, D. P.; McLafferty, F. W. Isotopic Assignment in Large-Molecule Mass Spectra by Fragmentation of a Selected Isotopic Peak. *Anal. Chem.* **1996**, *68* (3), 542–5.
- (5) Smith, D. F.; Blakney, G. T.; Beu, S. C.; Anderson, L. C.; Weisbrod, C. R.; Hendrickson, C. L. Ultrahigh Resolution Ion Isolation by Stored Waveform Inverse Fourier Transform 21 T Fourier Transform Ion Cyclotron Resonance Mass Spectrometry. *Anal. Chem.* **2020**, *92* (4), 3213–3219.
- (6) van Agthoven, M. A.; Lam, Y. P. Y.; O'Connor, P. B.; Rolando, C.; Delsuc, M.-A. Two-dimensional mass spectrometry: new perspectives for tandem mass spectrometry. *Eur. Biophys. J.* **2019**, *48* (3), 213–229.
- (7) van Agthoven, M. A.; O'Connor, P. B. Two-dimensional mass spectrometry in a linear ion trap, an in silico model. *Rapid Commun. Mass Spectrom.* **2017**, *31* (8), 674–684.
- (8) Snyder, D. T.; Szalwinski, L. J.; Wells, J. M.; Cooks, R. G. Logical MS/MS scans: a new set of operations for tandem mass spectrometry. *Analyst* **2018**, *143* (22), 5438–5452.
- (9) Szalwinski, L. J.; Holden, D. T.; Morato, N. M.; Cooks, R. G. 2D MS/MS Spectra Recorded in the Time Domain Using Repetitive Frequency Sweeps in Linear Quadrupole Ion Traps. *Anal. Chem.* **2020**, *92* (14), 10016–10023.
- (10) Snyder, D. T.; Szalwinski, L. J.; St. John, Z.; Cooks, R. G. Two-Dimensional Tandem Mass Spectrometry in a Single Scan on a Linear Quadrupole Ion Trap. *Anal. Chem.* **2019**, *91* (21), 13752–13762.
- (11) Szalwinski, L. J.; Cooks, R. G. Complex mixture analysis by two-dimensional mass spectrometry using a miniature ion trap. *Talanta Open* **2021**, *3*, 100028.
- (12) Driver, T.; Averbukh, V.; Frasiński, L. J.; Marangos, J. P.; Edelson-Averbukh, M. Two-Dimensional Partial Covariance Mass Spectrometry for the Top-Down Analysis of Intact Proteins. *Anal. Chem.* **2021**, *93* (31), 10779–10788.
- (13) Driver, T.; Cooper, B.; Ayers, R.; Pipkorn, R.; Patchkovskii, S.; Averbukh, V.; Klug, D. R.; Marangos, J. P.; Frasiński, L. J.; Edelson-Averbukh, M. Two-Dimensional Partial-Covariance Mass Spectrometry of Large Molecules Based on Fragment Correlations. *Physical Review X* **2020**, *10* (4), 041004.
- (14) Driver, T.; Bachhawat, N.; Frasiński, L. J.; Marangos, J. P.; Averbukh, V.; Edelson-Averbukh, M. Chimera Spectrum Diagnostics for Peptides Using Two-Dimensional Partial Covariance Mass Spectrometry. *Molecules* **2021**, *26* (12), 3728.
- (15) Pfändler, P.; Bodenhausen, G.; Rapin, J.; Houriet, R.; Gäumann, T. Two-dimensional Fourier transform ion cyclotron resonance mass spectrometry. *Chem. Phys. Lett.* **1987**, *138* (2–3), 195–200.
- (16) Pfändler, P.; Bodenhausen, G.; Rapin, J.; Walser, M. E.; Gäumann, T. Broad-band two-dimensional Fourier transform ion cyclotron resonance. *J. Am. Chem. Soc.* **1988**, *110* (17), 5625–5628.
- (17) Bensimon, M.; Zhao, G.; Gäumann, T. A method to generate phase continuity in two-dimensional Fourier transform ion cyclotron resonance mass spectrometry. *Chem. Phys. Lett.* **1989**, *157* (1–2), 97–100.
- (18) van Agthoven, M. A.; Chiron, L.; Coutouly, M.-A.; Sehgal, A. A.; Pelupessy, P.; Delsuc, M.-A.; Rolando, C. Optimization of the discrete pulse sequence for two-dimensional FT-ICR mass spectrometry using infrared multiphoton dissociation. *Int. J. Mass Spectrom.* **2014**, *370* (0), 114–124.
- (19) van Agthoven, M. A.; Lynch, A. M.; Morgan, T. E.; Wootton, C. A.; Lam, Y. P. Y.; Chiron, L.; Barrow, M. P.; Delsuc, M.-A.; O'Connor, P. B. Can Two-Dimensional IR-ECD Mass Spectrometry Improve Peptide de Novo Sequencing? *Anal. Chem.* **2018**, *90* (5), 3496–3504.
- (20) Marzullo, B. P.; Morgan, T. E.; Wootton, C. A.; Perry, S. J.; Saeed, M.; Barrow, M. P.; O'Connor, P. B. Advantages of Two-Dimensional Electron-Induced Dissociation and Infrared Multiphoton Dissociation Mass Spectrometry for the Analysis of Agrochemicals. *Anal. Chem.* **2020**, *92* (17), 11687–11695.
- (21) Marzullo, B. P.; Morgan, T. E.; Theisen, A.; Haris, A.; Wootton, C. A.; Perry, S. J.; Saeed, M.; Barrow, M. P.; O'Connor, P. B. Combining Ultraviolet Photodissociation and Two-Dimensional Mass Spectrometry: A Contemporary Approach for Characterizing Singly Charged Agrochemicals. *Anal. Chem.* **2021**, *93* (27), 9462–9470.
- (22) Chiron, L.; Coutouly, M.-A.; Starck, J.-P.; Rolando, C.; Delsuc, M.-A. SPIKE a processing software dedicated to Fourier spectroscopies. *arXiv (Computational Physics)*, 1608.06777, ver. 1, 2016, <https://arxiv.org/abs/1608.06777> (accessed June 2021).
- (23) Chiron, L.; van Agthoven, M. A.; Kieffer, B.; Rolando, C.; Delsuc, M.-A. Efficient denoising algorithms for large experimental datasets and their applications in Fourier transform ion cyclotron resonance mass spectrometry. *Proc. Natl. Acad. Sci. U. S. A.* **2014**, *111* (4), 1385–1390.
- (24) Bray, F.; Bouclon, J.; Chiron, L.; Witt, M.; Delsuc, M.-A.; Rolando, C. Nonuniform Sampling Acquisition of Two-Dimensional Fourier Transform Ion Cyclotron Resonance Mass Spectrometry for

Increased Mass Resolution of Tandem Mass Spectrometry Precursor Ions. *Anal. Chem.* **2017**, *89* (17), 8589–8593.

(25) Simon, H. J.; van Agthoven, M. A.; Lam, P. Y.; Floris, F.; Chiron, L.; Delsuc, M. A.; Rolando, C.; Barrow, M. P.; O'Connor, P. B. Uncoiling collagen: a multidimensional mass spectrometry study. *Analyst* **2016**, *141* (1), 157–165.

(26) Floris, F.; van Agthoven, M.; Chiron, L.; Soulby, A. J.; Wootton, C. A.; Lam, Y. P. Y.; Barrow, M. P.; Delsuc, M.-A.; O'Connor, P. B. 2D FT-ICR MS of Calmodulin: A Top-Down and Bottom-Up Approach. *J. Am. Soc. Mass Spectrom.* **2016**, *27* (9), 1531–1538.

(27) van Agthoven, M. A.; Wootton, C. A.; Chiron, L.; Coutouly, M.-A.; Soulby, A.; Wei, J.; Barrow, M. P.; Delsuc, M.-A.; Rolando, C.; O'Connor, P. B. Two-Dimensional Mass Spectrometry for Proteomics, a Comparative Study with Cytochrome c. *Anal. Chem.* **2016**, *88* (8), 4409–4417.

(28) Floris, F.; van Agthoven, M. A.; Chiron, L.; Wootton, C. A.; Lam, P. Y. Y.; Barrow, M. P.; Delsuc, M.-A.; O'Connor, P. B. Bottom-Up Two-Dimensional Electron-Capture Dissociation Mass Spectrometry of Calmodulin. *J. Am. Soc. Mass Spectrom.* **2018**, *29*, 207–210.

(29) Floris, F.; Vallotto, C.; Chiron, L.; Lynch, A. M.; Barrow, M. P.; Delsuc, M.-A.; O'Connor, P. B. Polymer Analysis in the Second Dimension: Preliminary Studies for the Characterization of Polymers with 2D MS. *Anal. Chem.* **2017**, *89* (18), 9892–9899.

(30) Paris, J.; Morgan, T. E.; Wootton, C. A.; Barrow, M. P.; O'Hara, J.; O'Connor, P. B. Facile Determination of Phosphorylation Sites in Peptides Using Two-Dimensional Mass Spectrometry. *Anal. Chem.* **2020**, *92*, 6817.

(31) Paris, J.; Morgan, T. E.; Marzullo, B. P.; Wootton, C. A.; Barrow, M. P.; O'Hara, J.; O'Connor, P. B. Two-Dimensional Mass Spectrometry Analysis of IgG1 Antibodies. *J. Am. Soc. Mass Spectrom.* **2021**, *32* (7), 1716–1724.

(32) Morgan, T. E.; Wootton, C. A.; Marzullo, B.; Paris, J.; Kerr, A.; Ellacott, S. H.; van Agthoven, M. A.; Barrow, M. P.; Bristow, A. W. T.; Perrier, S.; O'Connor, P. B. Characterization Across a Dispersity: Polymer Mass Spectrometry in the Second Dimension. *J. Am. Soc. Mass Spectrom.* **2021**, *32* (8), 2153–2161.

(33) van Agthoven, M. A.; Kilgour, D. P. A.; Lynch, A. M.; Barrow, M. P.; Morgan, T. E.; Wootton, C. A.; Chiron, L.; Delsuc, M.-A.; O'Connor, P. B. Phase relationships in two-dimensional mass spectrometry. *J. Am. Soc. Mass Spectrom.* **2019**, *30* (12), 2594–2607.

(34) Delsuc, M.-A.; Breuker, K.; van Agthoven, M. A. Phase Correction for Absorption Mode Two-Dimensional Mass Spectrometry. *Molecules* **2021**, *26* (11), 3388.

(35) Halper, M.; Delsuc, M.-A.; Breuker, K.; van Agthoven, M. A. Narrowband Modulation Two-Dimensional Mass Spectrometry and Label-Free Relative Quantification of Histone Peptides. *Anal. Chem.* **2020**, *92* (20), 13945–13952.

(36) Taucher, M.; Breuker, K. Top-Down Mass Spectrometry for Sequencing of Larger (up to 61 nt) RNA by CAD and EDD. *J. Am. Soc. Mass Spectrom.* **2010**, *21* (6), 918–929.

(37) Caravatti, P.; Allemann, M. The infinity cell: a new trapped-ion cell with radiofrequency covered trapping electrodes for Fourier transform ion cyclotron resonance mass spectrometry. *Org. Mass Spectrom.* **1991**, *26* (5), 514–18.

(38) Tsybin, Y. O.; Quinn, J. P.; Tsybin, O. Y.; Hendrickson, C. L.; Marshall, A. G. Electron Capture Dissociation Implementation Progress in Fourier Transform Ion Cyclotron Resonance Mass Spectrometry. *J. Am. Soc. Mass Spectrom.* **2008**, *19* (6), 762–771.

(39) Ledford, E. B., Jr; Rempel, D. L.; Gross, M. L. Space charge effects in Fourier transform mass spectrometry. II. Mass calibration. *Anal. Chem.* **1984**, *56* (14), 2744–8.

(40) Guan, S.; Jones, P. R. A theory for two-dimensional Fourier-transform ion cyclotron resonance mass spectrometry. *J. Chem. Phys.* **1989**, *91* (9), 5291–5.

(41) Tsybin, Y. O.; Witt, M.; Baykut, G.; Kjeldsen, F.; Hakansson, P. Combined infrared multiphoton dissociation and electron capture dissociation with a hollow electron beam in Fourier transform ion

cyclotron resonance mass spectrometry. *Rapid Commun. Mass Spectrom.* **2003**, *17* (15), 1759–1768.

(42) Marshall, A. G.; Hendrickson, C. L.; Jackson, G. S. Fourier transform ion cyclotron resonance mass spectrometry: a primer. *Mass Spectrom. Rev.* **1998**, *17* (1), 1–35.

(43) Glasner, H.; Rimpl, C.; Micura, R.; Breuker, K. Label-free, direct localization and relative quantitation of the RNA nucleobase methylations m6A, m5C, m3U, and m5U by top-down mass spectrometry. *Nucleic Acids Res.* **2017**, *45* (13), 8014–8025.

(44) Nikolaev, E. N.; Miluchihin, N.; Inoue, M. Evolution of an ion cloud in a Fourier transform ion cyclotron resonance mass spectrometer during signal detection: its influence on spectral line shape and position. *Int. J. Mass Spectrom. Ion Processes* **1995**, *148* (3), 145–57.

(45) Nikolaev, E. N.; Heeren, R. M. A.; Popov, A. M.; Pozdnev, A. V.; Chingin, K. S. Realistic modeling of ion cloud motion in a fourier transform ion cyclotron resonance cell by use of a particle-in-cell approach. *Rapid Commun. Mass Spectrom.* **2007**, *21* (22), 3527–3546.

(46) Vladimirov, G.; Hendrickson, C. L.; Blakney, G. T.; Marshall, A. G.; Heeren, R. M. A.; Nikolaev, E. N. Fourier Transform Ion Cyclotron Resonance Mass Resolution and Dynamic Range Limits Calculated by Computer Modeling of Ion Cloud Motion. *J. Am. Soc. Mass Spectrom.* **2012**, *23* (2), 375–384.

(47) Nikolaev, E. N.; Boldin, I. A.; Jertz, R.; Baykut, G. Initial experimental characterization of a new ultra-high resolution FTICR cell with dynamic harmonization. *J. Am. Soc. Mass Spectrom.* **2011**, *22* (7), 1125–1133.

(48) Qi, Y.; Witt, M.; Jertz, R.; Baykut, G.; Barrow, M. P.; Nikolaev, E. N.; O'Connor, P. B. Absorption-mode spectra on the dynamically harmonized Fourier transform ion cyclotron resonance cell. *Rapid Commun. Mass Spectrom.* **2012**, *26* (17), 2021–2026.

(49) Nikolaev, E. N.; Jertz, R.; Grigoryev, A.; Baykut, G. Fine Structure in Isotopic Peak Distributions Measured Using a Dynamically Harmonized Fourier Transform Ion Cyclotron Resonance Cell at 7 T. *Anal. Chem.* **2012**, *84* (5), 2275–2283.

(50) Ruddy, B. M.; Beu, S. C.; Kaiser, N. K.; Hendrickson, C. L.; Marshall, A. G. Coulombic shielding during ion cyclotron excitation in FT-ICR mass spectrometry. *Int. J. Mass Spectrom.* **2011**, *301* (1–3), 220–223.

(51) Aizikov, K.; O'Connor, P. B. Use of the Filter Diagonalization Method in the Study of Space Charge Related Frequency Modulation in Fourier Transform Ion Cyclotron Resonance Mass Spectrometry. *J. Am. Soc. Mass Spectrom.* **2006**, *17* (6), 836–843.

(52) Tolmachev, A. V.; Robinson, E. W.; Smith, R. D.; Leach, F. E., III; Futrell, J. H.; Pasa-Tolic, L. A conceptual approach for FT-ICR cell harmonization utilizing external shim electrodes. *Int. J. Mass Spectrom.* **2012**, *325–327*, 45–50.

(53) Kozhinov, A. N.; Tsybin, Y. O. Filter Diagonalization Method-Based Mass Spectrometry for Molecular and Macromolecular Structure Analysis. *Anal. Chem.* **2012**, *84* (6), 2850–2856.